(Received 30 August 2023, Accepted 21 November 2023, Scheduled 13 December 2023)

A Miniaturized Frequency Selective Surface for GSM Shielding by Utilizing a Spiral Handshake Structure

Xianjun Sheng, Chen Gu, Ning Liu*, Hongwei Wang, and Xiangyan Liu

Dalian University of Technology, Dalian 116024, China

ABSTRACT: This paper aims to design a compact frequency selective surface (FSS) for electromagnetic shielding in the 1.8 GHz band of GSM, ensuring that the stopband width covers the target frequency range in both simulations and actual measurements. The primary focus of this paper is to design a compact FSS with good miniaturization for real-world applications. The proposed FSS structure is a single-layer double-sided structure. The regression models reflecting the mapping relationship between the resonant frequency and structural parameters are established to guide the design. An equivalent circuit model (ECM) is presented to clearly explain the working mechanism of the FSS. The unit size is only $0.038\lambda_0$, where λ_0 is the wavelength of the resonant frequency in free space. In addition, the proposed FSS provides stable performance under oblique angles of incidence for both TE and TM polarizations. An FSS prototype has been manufactured for verification.

1. INTRODUCTION

Recently, the widespread use of mobile phones worldwide, driven by rapid wireless and internet advancements, has brought about a concerning issue: electromagnetic interference (EMI) [1, 2, 4]. Based on the findings from references [3], the primary source of EMI posing a significant threat to electronic equipment security is the Global System for Mobile Communication (GSM) 1.8 GHz band (1.71–1.88 GHz), where many mobile phones operate. To address this issue, FSSs have been extensively investigated to offer efficient shielding [4].

FSSs are two-dimensional periodic structures and have been extensively studied for many years [5]. Due to their frequency-filtering characteristics, FSSs have found extensive utility in communication systems for the creation of antenna reflectors, spatial filters, electromagnetic shielding, and more [6–8]. While FSSs are theoretically infinite planar structures, practical applications often confine them to limited spaces. To preserve their desired frequency-filtering characteristics in practical scenarios, it becomes imperative to miniaturize the constituent elements [5]. Hence, designing miniaturized FSS for certain application scenarios has consistently remained a popular research direction.

A compact dual-band FSS for GSM shielding by utilizing a 2.5-dimensional structure was presented in [4]. A miniaturized meandered structure with a thin dielectric plate that provides a stopband for GSM at 1.8 GHz band was presented in [9]. A miniaturized FSS with stable response for WLAN applications was presented in [10].

In this paper, a miniaturized FSS based on Archimedean spiral handshake is proposed. The primary aim of this study is to devise a compact band-stop FSS that can effectively attenuate the transmission of signals within the 1.8 GHz band of GSM. Compared to the aforementioned structures, the proposed structure has a smaller unit size at the resonant frequency. To verify the design, a physical sample has been fabricated and measured.

* Corresponding author: Ning Liu (liun@dlut.edu.cn).

2. FSS DESIGN

As shown in Fig. 1(a), the FSS structure is a single-layer double-sided structure. The stripes in the bottom layer unit are rotated by 90° relative to the stripes in the top layer to achieve polarization stability. Fig. 1(b) shows how the strips of adjacent cells are connected. The strips were designed by Archimedes spiral. The equation of the Archimedean spiral in the Cartesian coordinate system is:

$$\begin{cases} x(t) = (A + Bt)\cos(t) \\ y(t) = (A + Bt)\sin(t) \end{cases} \tag{1}$$

In this study, the two metallic arrays are mounted on the two sides of an F4B-2 substrate with a thickness of $h = 0.5$ mm, a permittivity of $\varepsilon_r = 2.65$, a tangent loss of $\tan\delta = 0.005$, and a unit cell period of $D = 6.4$ mm.

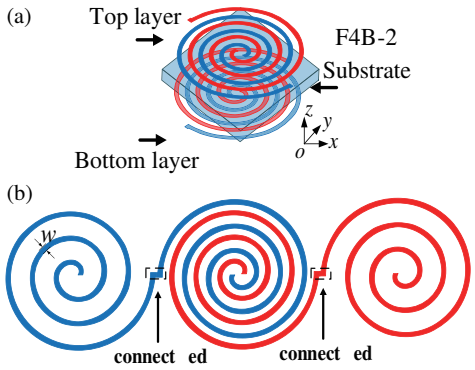

FIGURE 1. Geometry of the spiral handshake FSS. (a) Overview. (b) Connection method.

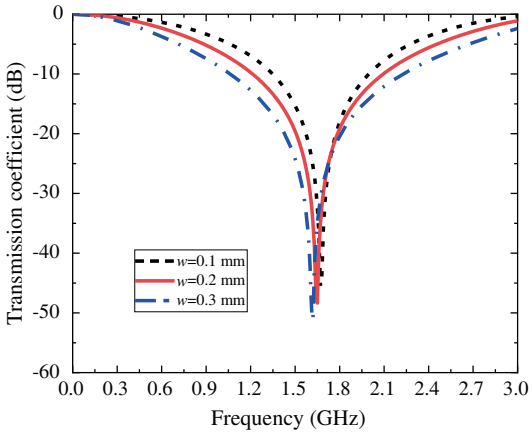

FIGURE 2. Effects of strip width w on the transmission coefficient.

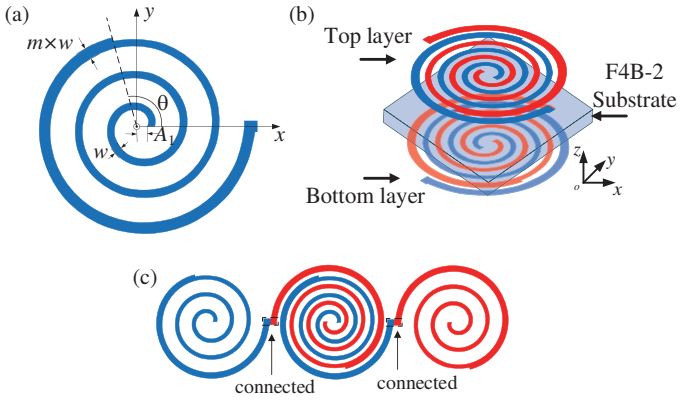

FIGURE 3. Geometry of the proposed FSS. (a) Overview. (b) Two-section spiral strip. (c) Connection method.

When simulating in CST, it was observed from Fig. 2 that changing the strip width 'w' of this structure did not lead to significant variations in its performance. Therefore, to enhance the tunability of the structure, a two-strip configuration with unequal widths is considered.

As shown in Fig. 3(a), the "one hand" of the structure is composed of two spiral strips with different widths. The thinner strip on the inner ring is the first metal strip, and the thicker outer ring strip is the second metal strip. The width of the outer ring strip is m times that of the inner ring strip, i.e., $m{\times}w$. Thus, the strip width ratio m determines the relationship between the widths of the two segments of the spiral. Meanwhile, the upper bound te_1 of parameter t for the first section of the spiral strips determines the length of each segment of the two spirals. The spiral parameter A_1 can also be adjusted as a tunable parameter. The overview of the structure is shown in Fig. 3(b).

According to the subsequent regression analysis, it can be inferred that both te_1 and A_1, as adjustable parameters, are capable of significantly altering the resonant frequency of the structure when they vary. Fig. 3(c) shows how the strips of adjacent cells are connected. The combination of the two spiral strips exhibits a stable filtering characteristic.

For the proposed FSS structure, four main parameters are easy to adjust and play an important role in the filtering characteristics. These parameters include the unit period D, the ratio m of the width of the metal strips, the parameters $A_{1,}$, and the upper bound te_1 of parameter t for the first section of the spiral. For example, in Fig. 3(a), $te_1 = 4\pi + \theta$.

In this paper, D is 6.4 mm; w is 0.2 mm; and m is 1.5. At this time, the width of the second part of the metal strip is 0.3 mm. The two metallic arrays are mounted on the two sides of an F4B-2 substrate with a thickness of $h = 0.5$ mm, a permittivity of $\varepsilon_r = 2.65$, and a tangent loss of $\tan\delta = 0.005$.

Regression analysis is applied to investigate the correlation between the remaining two parameters, namely A_1 and te_1, and the resonate frequency f_1. This allows for guiding the subsequent adjustments to the structural parameters for frequency regulation.

To build a regression model, the first step is to collect some data. Experiments were conducted in CST using A_1 and te_1 as independent variables, and f_1 as dependent variables. Due to the finite nature of the unit cell period D in the plane, there are inherent constraints on the geometric sizes of its internal shape during the design process. In this study, the selected ranges for A_1 and te_1 are A_1: 0.1–0.4 mm and te_1: 0.1–15 rad. This will result in a range for f_1, ranging from 1.50 to 1.82 GHz.

Figure 4 shows the scatter plots and fitting surface plots. As shown in the figure, once te_1 is determined, f_1 will decrease with the increase of A_1. The expression of the regression model is in Eq. (2).

$$\begin{aligned} f_1(x,y) &= p_{00} + p_{10}x + p_{01}y + p_{20}x^2 + p_{11}xy + p_{02}y^2 \\ &\quad + p_{30}x^3 + p_{21}x^2y + p_{12}xy^2 + p_{03}y^3 \end{aligned} \tag{2}$$

Where $p_{00} = 1.722$, $p_{10} = -0.3647$, $p_{01} = -0.01533$, $p_{20} = -0.8802$, $p_{11} = 0.01523$, $p_{02} = 0.005077$, $p_{30} = 1.431$, $p_{21} = 0.00515$, $p_{12} = -0.001083$, $p_{03} = -0.0002281$; x represents A_1, y represents te_1, and $f_1(x,y)$ represents f_1.

For the required f_1, the structural parameters A_1 and te_1 can be inversely calculated according to the above equation. For example, substitute $f_1 = 1.8$ GHz into the equation to calculate and take a group of appropriate solutions: $A_1 = 0.16$ mm, $te_1 = 14.43$ rad. Use this result to modify the CST model, and its S_{21} curve shown in Fig. 5 can be obtained. It can be seen that the regression model plays a crucial role in this design process. The FSS exhibits 1.07 GHz bandwidths with an insertion loss of less than -10 dB around the central frequency of 1.79 GHz. These performance metrics align with the design objectives of attenuating signal transmission within the 1.71–1.88 GHz band of GSM.

The working mechanism of the FSS can be intuitively understood by building the ECM of the FSS. For TE polarization, the surface current and electric field distribution diagrams of the unit at $f_1 = 1.79$ GHz are presented in Fig. 6.

It can be seen from the figure that at f_1, the outer ring metal strip of the top unit forms the inductance Lt_1. The metal strip of the middle ring forms the inductance Lt_2. The metal strip gap of the outer ring forms the capacitance Ct_1 in parallel with

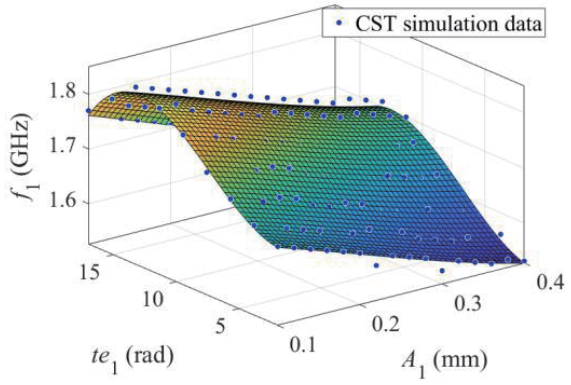

FIGURE 4. Sample points and fitting surfaces.

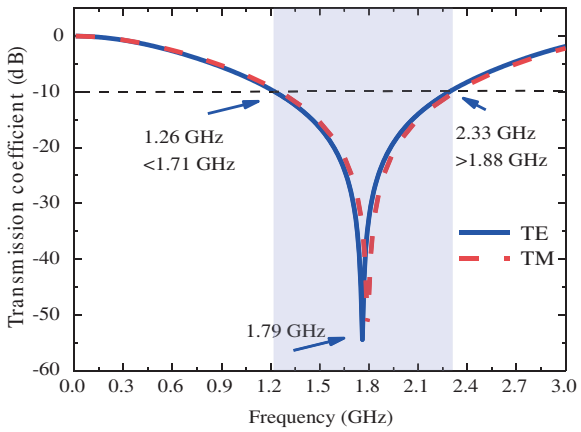

FIGURE 5. Transmission curve of the FSS guided by the models.

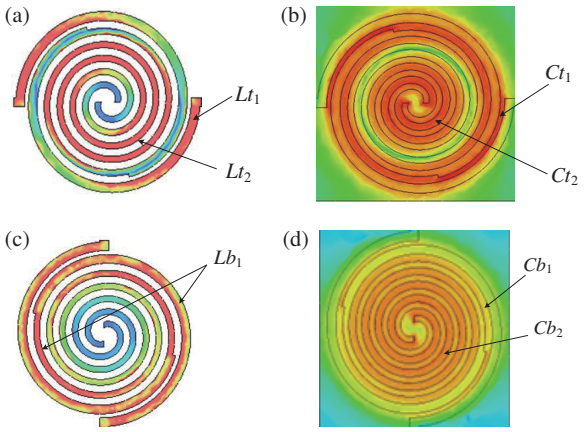

FIGURE 6. Surface current and electric field diagram of the array at $f_1 = 1.79$ GHz. (a) Surface current of the top array. (b) The electric field of the top array. (c) Surface current of the bottom array. (b) The electric field of the bottom array.

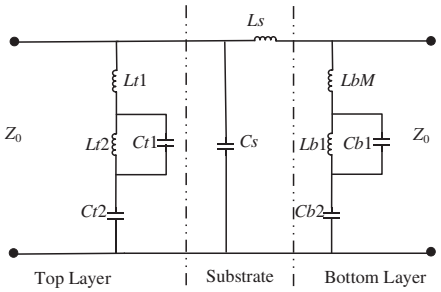

FIGURE 7. The ECM of the proposed FSS. ($Lt1 = 1.0$ nH, $Lt2 = 17.6$ nH, $Ct1 = 0.073$ pF, $Ct2 = 0.36$ pF, $Ls = 0.00063$ nH, $Cs = 0.006$ pF, $LbM = 2.53$ nH, $Lb1 = 5.7$ nH, $Cb1 = 0.37$ pF, $Cb2 = 0.785$ pF).

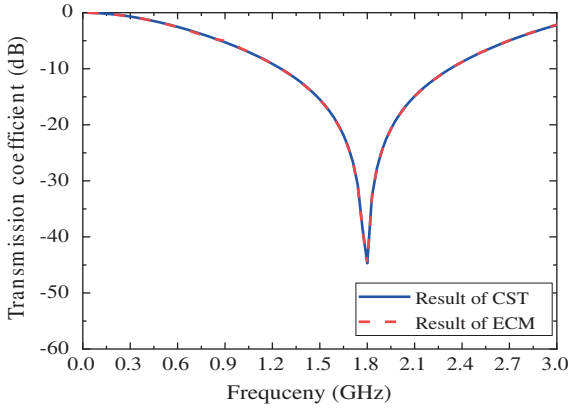

FIGURE 8. Comparison between the transmission coefficient of ECM and CST simulation results.

Lt_2. The gap in the innermost ring and inner ring forms the capacitance Ct_2.

The substrate is characterized by a shunt capacitance (Cs) and a series inductance (Ls). The value of the shunt capacitance, Cs, is determined using the formula $\varepsilon_0\varepsilon_r h/2$, where ε_0 represents the permittivity of free space, ε_r is the relative permittivity of the substrate, and h denotes the height of the substrate. Likewise, the value of the series inductance, Ls, is calculated using the formula $\mu_0\mu_r h$, where μ_0 stands for the permeability of free space, and μ_r signifies the relative permeability of the substrate [11].

The outer ring metal strip of the bottom unit forms the inductance Lb_1 in TE mode. Since the current path of this frequency point is long and connected with the current path of adjacent units, it is necessary to consider the mutual inductance Lb_M between adjacent units [12]. The metal strip gap of the outer ring forms the capacitance Cb_1 in parallel with Lb_1. The gap in the intermediate ring and the inner ring forms the capacitance Cb_2 connected in series with Lb_1.

Subsequently, the ECM was established preliminarily in advanced design system (ADS), and, with CST's S_{21} as the target, the ECM component values were fine-tuned, and the ECM's S_{21} was calculated. If the component parameters are suitable (generally, in the L-C band, the inductance value for meandering structures falls within the range of 1–30 nH, and the capacitance typically ranges from 0.01–2 pF [5, 13]), and the S_{21} gen-

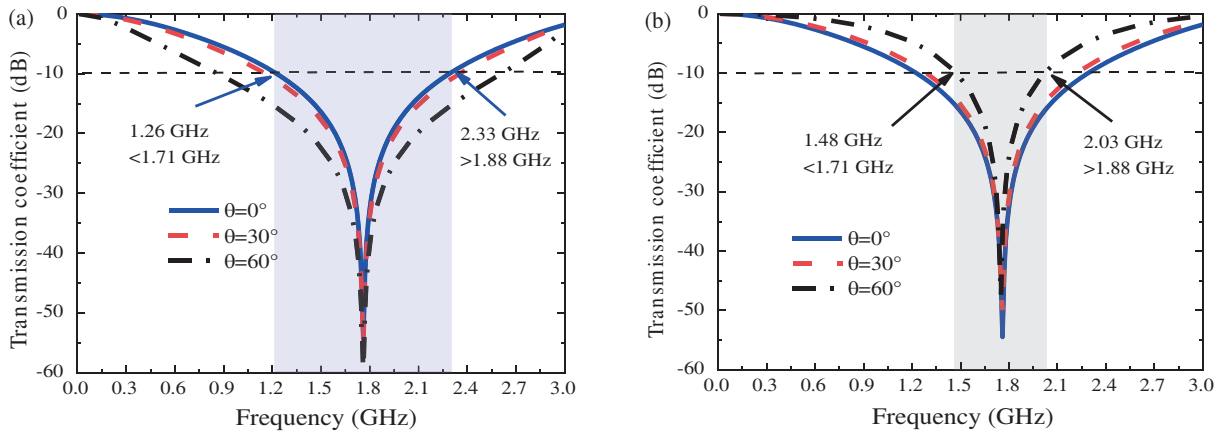

FIGURE 9. Transmission coefficients of the proposed FSS structure under oblique incidence. (a) TE polarization. (b) TM polarization.

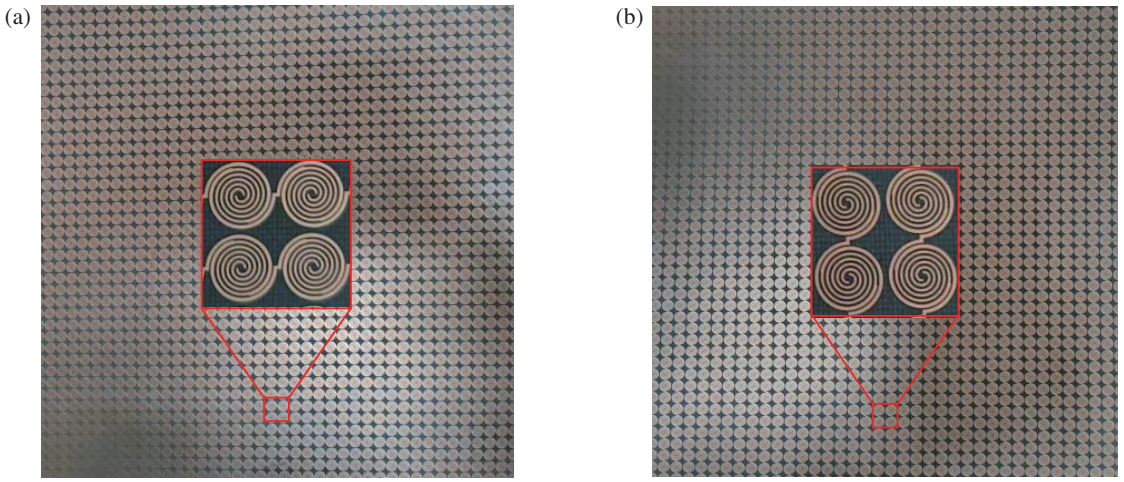

FIGURE 10. Images of the manufactured FSS prototype. (a) Top units. (b) Bottom units.

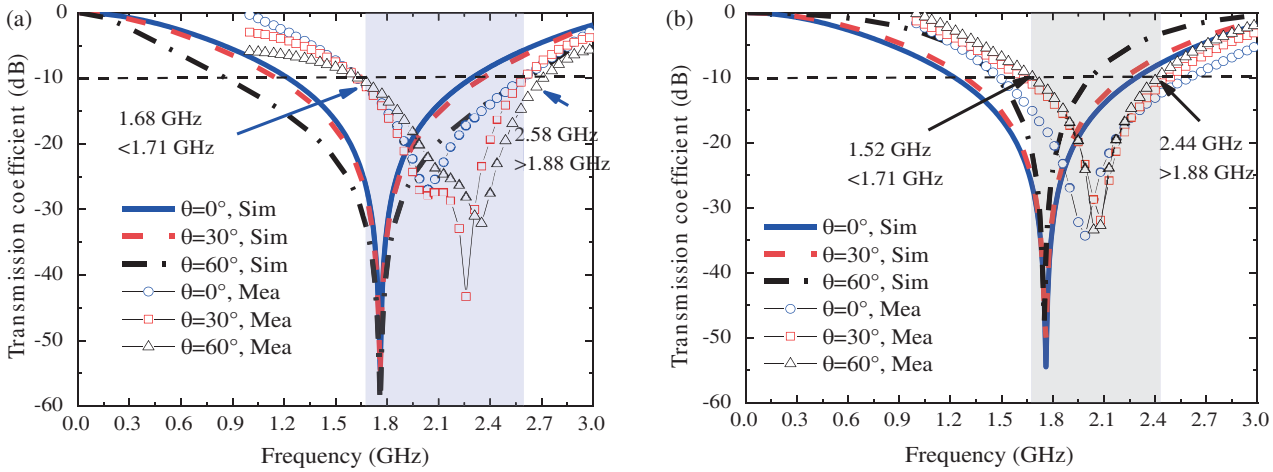

FIGURE 11. Comparisons between the simulated and the measured results: (a) TE polarization. (b) TM polarization.

erated by the ECM closely matches the S_{21} provided by CST, it indicates that the ECM can effectively characterize the corresponding FSS.

The preliminary ECM established is shown in Fig. 7, and the tuning results are indicated in the figure caption. According to Fig. 8, it can be observed that the preliminary ECM is accurate. Furthermore, after tuning, the ECM effectively characterizes the FSS.

Figure 9 shows the transmission coefficient of the proposed FSS under different incident angles and different polarizations.

It can be seen that under two polarization modes when incident angle θ changes from 0° to 60°, the FSS can always form a stopband with a certain bandwidth around 1.8 GHz for GSM.

Finally, the comparisons with similar works mentioned above were made in Table 1. Article [4] designed a dual-band FSS for GSM using a 2.5D structure, achieving a miniaturization of $0.072\lambda_0$. Article [9] employed a meandering structure to design a single-band FSS for GSM with a miniaturization of $0.045\lambda_0$. Article [10] also used a meandering structure to design a dual-band FSS for WiFi, achieving a miniaturization of $0.11\lambda_0$. These three articles share a similar focus with our paper, as they all aim to fulfill specific practical applications. Article [13] designed a meandering structure and achieved an excellent miniaturization of $0.028\lambda_0$. While its work has more theoretical implications, it may currently lack matching real-world applications. Our paper starts with the goal of shielding GSM signals in the 1.8 GHz band and designs an FSS with a miniaturization effect of $0.038\lambda_0$. Compared to articles [4, 9, 10], it offers a better miniaturization effect. In contrast to article [13], it caters to a specific application scenario.

TABLE 1. Comparisons to similar works.

Ref	ε_r	Unit size	Band	Angle
[4]	3.2	$0.072\lambda_0$	Dual	60°
[9]	3.2	$0.045\lambda_0$	Single	60°
[10]	2.65	$0.11\lambda_0$	Single	60°
[13]	2.65	$0.028\lambda_0$	Single	60°
This FSS	2.65	$0.038\lambda_0$	Single	60°

3. MEASUREMENT

For additional validation, as depicted in Fig. 10, an FSS prototype comprising 60×60 elements was manufactured on an F4B-2 substrate through conventional printed circuit board fabrication techniques. The structural characteristics of the fabricated FSS align precisely with the previously mentioned design parameters.

The measurement setup primarily consists of the following components: transmitting and receiving antennas, antenna mounts, a vector network analyzer, and wave-absorbing foam, among others. Before measurement, mechanical calibration of the instrument is performed, and the time-domain gate technique is applied to eliminate diffraction waves [14]. Variations in measurements involving different polarizations and incident angles are accomplished by adjusting the orientations of both the antennas and the FSS prototype. Additional information is available in reference [15].

The measured transmission coefficients of the fabricated FSS under different incident angles, together with the simulated ones, are shown in Fig. 11. There are certain acceptable deviations between the measurement results and simulation outcomes. This is mainly caused by the deviation of the dielectric constant of the dielectric substrate and measurement error. However, it can be observed that the measurement results can still meet the above application scenarios.

4. CONCLUSION

In this paper, a miniaturized FSS is proposed to provide a stopband for the 1.8 GHz band of GSM. The simulated and experimental results verify that this two-sided structure of the Archimedean spiral handshake can achieve high miniaturization and polarization stability. Regression models for some structural parameters and resonant frequency are established to guide the design process. An ECM has been established to clearly explain the working mechanism of the FSS. The sample's performance can meet the application scenarios.

ACKNOWLEDGEMENT

This work was supported by the National Natural Science Foundation of China under Grant Nos. 52005079 and 52075069, and by the Fundamental Research Funds for the Central Universities under Grant No. DUT21RC(3)069.

REFERENCES

[1] Periyasamy, M. and R. Dhanasekaran, "Electromagnetic interference on critical medical equipments by rf devices," *Proc. Int. Conf. Electron. Comput. Technol.*, 78–82, April 3–5 2013.

[2] Kaur, M., S. Kakar, and D. Mandal, "Electromagnetic interference," *Proc. Int. Conf. Electron. Comput. Technol.*, Vol. 4, No. 1, 1–5, 2011.

[3] Unal, E., A. Gokcen, and Y. Kutlu, "Effective electromagnetic shielding," *IEEE Microwave Magazine*, Vol. 7, No. 4, 48–54, Aug. 2006.

[4] Yin, W., H. Zhang, T. Zhong, and X. Min, "A novel compact dual-band frequency selective surface for gsm shielding by utilizing a 2.5-dimensional structure," *IEEE Transactions on Electromagnetic Compatibility*, Vol. 60, No. 6, 2057–2060, Dec. 2018.

[5] Liu, N., X. Sheng, C. Zhang, J. Fan, and D. Guo, "A miniaturized triband frequency selective surface based on convoluted design," *IEEE Antennas And Wireless Propagation Letters*, Vol. 16, 2384–2387, 2017.

[6] Mittra, R., C. H., and T. Cwik, "Techniques for analyzing frequency selective surfaces - a review," *Proceedings of the IEEE*, Vol. 76, No. 12, 1593–1615, Dec. 1988.

[7] Ranga, Y., L. Matekovits, K. Esselle, and A. Weily, "Multioctave frequency selective surface reflector for ultrawideband antennas," *IEEE Antennas and Wireless Propagation Letters*, Vol. 10, 219–222, 2011.

[8] Syed, I., Y. Ranga, L. Matekovits, K. Esselle, and S. Hay, "A single-layer frequency-selective surface for ultrawideband electromagnetic shielding," *IEEE Transactions on Electromagnetic Compatibility*, Vol. 56, No. 6, 1404–1411, Dec. 2014.

[9] Dewani, A., S. O'Keefe, D. Thiel, and A. Galehdar, "Miniaturised meandered square frequency selective surface on a thin flexible dielectric with selective transmission," *Flexible and Printed Electronics*, Vol. 1, No. 2, 025001, Jun. 1 2016.

[10] Natarajan, R., M. Kanagasabai, S. Baisakhiya, R. Sivasamy, S. Palaniswamy, and J. Pakkathillam, "A compact frequency selective surface with stable response for wlan applications," *IEEE Antennas and Wireless Propagation Letters*, Vol. 12, 718–720, 2013.

[11] Mellita, R., D. Chandu, S. Karthikeyan, and P. Damodharan, "A miniaturized wideband frequency selective surface with interconnected cell structure," *Aeu-international Journal of Elec-*

tronics and Communications, Vol. 120, Jun. 2020.

[12] Zhao, P.-C., Z.-Y. Zong, W. Wu, and D.-G. Fang, "A convoluted structure for miniaturized frequency selective surface and its equivalent circuit for optimization design," *IEEE Transactions on Antennas and Propagation*, Vol. 64, No. 7, 2963–2970, Jul. 2016.

[13] Hong, T., K. Peng, and M. Wang, "Miniaturized frequency selective surface using handshake convoluted stripe," *IEEE Antennas and Wireless Propagation Letters*, Vol. 18, No. 10, 2026–2030, Oct. 2019.

[14] Sheng, X., X. Zhao, N. Liu, and X. Gao, "Design of miniaturized fss using equivalent circuit model and multi-objective particle swarm optimization," *Journal of Physics D-applied Physics*, Vol. 54, No. 40, 405001, Oct. 7 2021.

[15] Liu, N., X. Sheng, and X. Zhao, "Design of dual-polarized frequency selective rasorber with two independent transmission windows using multi-resonators," *IEEE Access*, Vol. 8, No. 99, 223 723–223 729, 2020.